

COMPARISON OF MSG/SEVIRI CALIBRATION REFERENCE WITH MERIS BRF OVER BRIGHT DESERT CALIBRATION TARGETS

Y.M. Govaerts⁽¹⁾, M. Clerici⁽²⁾

⁽¹⁾ EUMETSAT, Postfach 10 05 55, D-64295 Darmstadt, Germany Fax: +49 (0)6151 807-838

⁽²⁾ SC, Milano, Italy

ABSTRACT

Meteosat Second Generation (MSG) is the new generation of European geostationary meteorological satellites operated at EUMETSAT. SEVIRI, the MSG main radiometer, measures the reflected solar radiation within three spectral bands centered at 0.6, 0.8 and 1.6 μm , and within a broad band similar to the VIS channel of MVIRI, the radiometer on-board the first generation of METEOSAT satellites. The operational calibration of these channels relies on modelled reflectances over bright desert sites, as no in-flight calibration device is available. These simulated reflectances represent therefore the “reference” against which SEVIRI is calibrated. The present study evaluates the uncertainties associated with the characterization of this “reference”, *i.e.*, the modelled reflectances. To this end, top-of-atmosphere simulated reflectances are compared with calibrated space-borne observations acquired over the SEVIRI desert calibration sites. Results show that the relative bias between simulation and observation does not exceed $\pm 6\%$.

1 INTRODUCTION

Meteosat Second Generation (MSG) is a new series of European geostationary meteorological satellites operated by EUMETSAT. The MSG programme consists of at least three satellites each with an expected lifetime of seven years. The first one has been successfully launched in August 2002. MSG is a spinning satellite, carrying a twelve channel imager, called SEVIRI (Spinning Enhanced Visible and Infrared Imager). The characteristics of this instrument are briefly described in the next Section. As no on-board calibration device is available for the solar channels, their calibration has to rely on vicarious methods. Any calibration method requires first of all the definition and characterization of an independent “calibration reference”. The choice of this reference is discussed in [5] and has been driven by the need to fulfill the accuracy and precision requirements of the MSG operational ground segment during the entire duration of the mission, *i.e.*, more than 12 years.

SEVIRI solar channels calibration reference consists of simulated Top-Of-Atmosphere (TOA) Bidirectional Reflectance Factor (BRF) generated in the 0.3 - 1.8 μm spectral region over bright desert targets. Radiative transfer simulations are performed with the 6S code [14] using a data set of surface and atmospheric properties. This data set is used to simulate SEVIRI observations accounting for the exact viewing and illumination conditions as well as the spectral characteristics of the instrument. The duration of the MSG mission prohibits the continuous characterization of a limited number of targets with ground observations. The proposed strategy relies therefore on the definition of a large number of stable targets for which the surface properties are estimated once and for all. The objective of this paper is to establish the accuracy (*i.e.*, bias) and precision (*i.e.*, variance) of this reference. The proposed method relies on the comparison between simulations and calibrated observations acquired by spaceborne instruments. To this end, Envisat/MERIS, ERS2/ATSR-2, SeaStar/SeaWiFS and VEGETATION data have been collected over the calibration targets. These data have next been simulated accounting for the actual observation conditions of each instrument. This analysis shows that the monthly mean relative bias between observation and simulation averaged over all targets remains below 6%. It also reveals some differences between these instruments.

2 THE SEVIRI RADIOMETER

SEVIRI is the main radiometer on-board the MSG spacecraft. It scans the Earth disc every 15 minutes within 11 spectral channels located between $0.6\mu\text{m}$ and $14\mu\text{m}$ and a high resolution broadband visible channel (HRV). The East-West and North-South sampling distance at the sub-satellite point is $3\times 3\text{ km}$ ($1\times 1\text{ km}$ for HRV), and the instantaneous field of view is about 5 km (2 km for HRV). The characteristics of the channels located in the solar spectral region are given in Table 1, where the actual pre-launch radiometric performance are given for the SEVIRI instrument on-board MSG-1. Each spectral channel is composed of three detectors, but HRV with nine. The output signal of all channels is coded on 10 bits. The medium-term (long-term) drift is expected to be better or equal to 0.1% (2%) of the maximum dynamic range. The normalized spectral response $\xi(\lambda)$ of the solar channels are characterized with a mean relative error of about 1% . The radiometric pre-processing of level 1.0 data, *i.e.*, the transformation of raw data to level 1.5 geo-located radiances, includes the linearisation of the signal, the equalization of the detector output of a same channel and finally the pixel geo-location to a reference grid centered at 0 degree longitude [11]. The geo-location absolute accuracy is expected to be about one pixel and a root mean square error from image to image less than 0.5 pixel.

Table 1: SEVIRI Solar Channel Characteristics. The dynamic range is given in $\text{Wm}^{-2}\text{sr}^{-1}\mu\text{m}^{-1}$. The Signal to Noise Ratio (SNR) is given at 1% of the maximum dynamic range. The standard deviation (std. d.) of the Normalized Spectral Response (NSR) characterization error is given in percent. The calibration requirement is given in $\text{Wm}^{-2}\text{sr}^{-1}\mu\text{m}^{-1}$.

Channel	Spectral Band (μm)	Dynamic Range	Short-term Noise Perform.	NSR std. d.	Cal. Requ.
HRV	0.37 – 1.25	0 – 460	SNR > 4.6	1.8%	9.18
VIS0.6	0.56 – 0.71	0 – 533	SNR > 14.3	1.0%	10.66
VIS0.8	0.74 – 0.88	0 – 357	SNR > 9.7	1.0%	7.14
NIR1.6	1.50 – 1.78	0 – 75	SNR > 3.0	0.8%	1.50

3 CALIBRATION REFERENCE CHARACTERIZATION

3.1 Reference Definition

The main reference for the calibration of the SEVIRI solar channels consists of simulated TOA spectral reflectances over bright desert targets. The spectral reflectance $r(\chi_d, \lambda; \chi_p)$ impinging on a spaceborne instrument at the wavelength λ is determined by a set of independent parameters $\{\chi_d\}$ that define the observation conditions and a set of state variables $\{\chi_p\}$ that describe the radiative properties of the observed targets, *i.e.*, the atmosphere and the underlying surface. The independent parameters include the sun and viewing angles, the time of observation, the location of the target and the finally the wavelength λ . Hence, the definition of the “calibration reference” essentially consists in the characterization of the state variables that control the transfer of radiation in the surface-atmosphere system. In order to minimize the characterization effort of the surface properties, the MSG mission lasts more than 12 years, it is preferable to select stable and uniform targets, as can be found in arid desert areas. Additionally, TOA reflectance over bright surfaces is not very sensitive to the presence of low aerosol load, which represents a decisive advantage in terms of the required characterization accuracy of the atmospheric properties.

A series of radiometrically stable and bright targets, located in the Saharan and Saudi Arabian deserts, have already been identified by [4]. These arid targets are large uniform areas, essentially consisting of sand dunes, gravel and rocks. The linear arrangement of sand dunes of some targets, characterized by [3], might be responsible for an azimuthal dissymmetry in the Bidirectional Reflectance Factor (BRF) between the left and the right part of the hemisphere with respect to the principal plane. [8] demonstrated that this dissymmetry does not exceed a few percents and is smoothed by the multiple scattering between the atmosphere and the surface, which is important over bright soils. Hence, the surface bidirectional reflectance is therefore represented by a simple model [9], coupled with 6S radiative transfer code [14]. This bare soil BRF model depends on three state variables, namely, the single scattering albedo ω_0 , the asymmetry of the phase function Θ and finally a porosity parameter h . The major atmospheric state variables controlling TOA reflectances over bright surfaces are the total column water vapor G_H , the total column ozone G_O and the aerosol optical thickness τ . A US62 vertical atmospheric profile and desert dust aerosol type [12] are assumed all year long. The characterization of these six state variables and associated errors are described in the next two Sections.

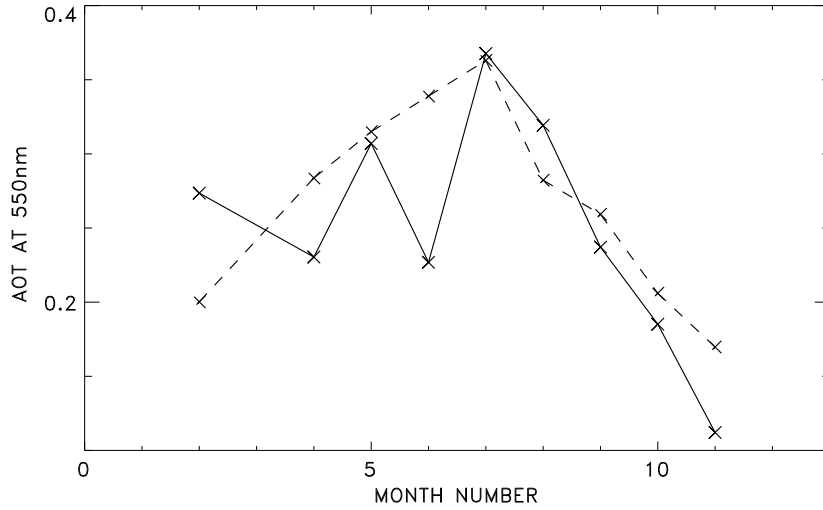


Figure 1: Monthly mean temporal profile of the AOT over the Solar Village AERONET site located in the Arabian desert. The solid line shows the ground-base measurement and of the dashed line the AOT climate data set based on TOMS AI.

3.2 Atmospheric Parameters

The calibration of SEVIRI solar channels takes place only when the atmosphere is perfectly clear [5]. Thus, the characterization of the atmospheric properties does not include cloudy and stand storm cases. Our major concern is to represent correctly the seasonal variations of the atmospheric state variables over the Saharan and Saudi Arabian deserts in order to minimize any possible temporal bias of the calibration reference. A monthly mean ozone climate data set has been built from 10 years of TOMS observations, with typical standard deviation of about 15%. The total column water vapor is taken from the European Centre for Medium-Range Weather Forecasts (ECMWF) analyzed data, which error does not exceed 10%. Aerosols have a limited impact on TOA reflectance over bright surfaces, except in case of severe dust events. As demonstrated by [2], TOMS absorbing Aerosol Index (AI) provides a good indication of the mineral dust distribution. A non-linear expression

$$\tau_{\lambda} = a(\lambda) + b(\lambda) \exp\left(\text{AI}^{c(\lambda)}\right) \quad (1)$$

is used to convert the TOMS AI into Aerosol Optical Thickness (AOT). The values of the coefficients $a(\lambda) = 0.055$, $b(\lambda) = 0.109$ and $c(\lambda) = 0.705$ were estimated inverting Eq. 1 against contemporaneous ground-based measurements at $0.440 \mu\text{m}$. These observations were extracted from the AERONET stations located nearby the Saharan and Arabian deserts. The Root Mean Square Error (RMSE) between the monthly mean ground-based AOT measurements and the collocated TOMS AI-based AOT is equal to 0.09, which corresponds to an average relative error of about 50%. Despite the limitations of this data set, it allows to account for the seasonal cycle of the AOT over desert areas as can be seen on Figure (1).

3.3 Surface Parameters

Only very limited ground measurements of the selected calibration target surface radiative properties exist [3]. In the framework of the SEVIRI calibration reference definition, it is necessary to characterize the surface spectral and directional properties at a spatial resolution of several kilometers. For that purpose, space-borne observations acquired by ADEOS-1/POLDER in the 0.443 , 0.670 , 0.765 and $0.865 \mu\text{m}$ spectral bands and ERS2/ATSR2 in the $1.6 \mu\text{m}$ band, corrected from atmospheric scattering and absorption effects were used. For each target, the surface BRDF model of [9] were inverted against atmospherically corrected observations with the genetic algorithm proposed by [10]. The errors $\varepsilon_{\omega_0}(\lambda_M)$, $\varepsilon_{\Theta}(\lambda_M)$, $\varepsilon_h(\lambda_M)$ of the best estimate of the state variables $\omega_0(\lambda_M)$, $\Theta(\lambda_M)$, $h(\lambda_M)$ in each spectral band λ_M of observation correspond to the standard deviation of all possible solutions fitting observations within a given accuracy. The calibration of SEVIRI solar channels requires the characterization of the surface properties from about $0.35 \mu\text{m}$ up to $1.8 \mu\text{m}$. It is therefore necessary to interpolate and extrapolate the state variables derived in each band λ_M at any desired wavelengths within that interval. In the 0.443 – $0.865 \mu\text{m}$ spectral interval, the surface

BRF field $r_s(\omega_0(\lambda_M), \Theta(\lambda_M), h(\lambda_M))$ is linearly interpolated at a desired wavelength λ , and the surface BRF model subsequently inverted against r_s to retrieve the values of $\omega_0(\lambda)$, $\Theta(\lambda)$, $h(\lambda)$ at that particular wavelength. Since the spectral variations of $\Theta(\lambda)$ and $h(\lambda)$ are small, it is assumed that only the estimated error $\varepsilon_\omega(\lambda)$ has to be increased due to the linear interpolation. The error $\varepsilon_\omega(\lambda)$ is estimated at wavelength λ with

$$\varepsilon_\omega(\lambda) = \sqrt{\varepsilon_\omega^2(\lambda_{M'}) + \left(\frac{\partial\omega_0(\lambda)}{\partial\lambda} \varepsilon_\lambda\right)^2}. \quad (2)$$

where $\lambda_{M'}$ is the POLDER band closest to the wavelength λ and ε_λ is equal to $(\lambda_{M'} - \lambda)/2$.

A different approach is adopted for the estimation of $\omega_0(\lambda)$, $\Theta(\lambda)$, $h(\lambda)$ outside the 0.443–0.865 μm interval. The proposed method is based on a comparison of the Directional Hemispherical Reflectance (DHR) estimated in each band λ_M with surface spectra of the ASTER spectral Library (<http://speclib.jpl.nasa.gov>). The ensemble of bright bare soil spectra $S(\lambda)$ of the ASTER spectral Library matching these five $\text{DHR}_0(\lambda_M)$ values are next identified. A mean surface spectrum $\bar{S}(\lambda)$ and standard deviation $\sigma_{\bar{S}}(\lambda)$ are calculated with all the spectra identified. The surface BRF field $r_s(\lambda)$ at any desired wavelength in the 0.350–0.443 μm and 0.865–1.80 μm regions is scaled in such a way that the corresponding $\text{DHR}_0(\lambda)$ is equal to the mean spectrum value $\bar{S}(\lambda)$. The corresponding scaled BRF field is next inverted to retrieve the value of $\omega_0(\lambda)$, $\Theta(\lambda)$, $h(\lambda)$ at that wavelength and the error $\varepsilon_\omega(\lambda)$ is estimated as

$$\varepsilon_\omega(\lambda) = \sqrt{\varepsilon_\omega^2(\lambda_{M'}) + \left(\frac{\sigma_{\bar{S}}(\lambda)}{\bar{S}(\lambda)} \omega_0(\lambda)\right)^2}. \quad (3)$$

These interpolation and extrapolation procedures are used for the estimation of $\omega_0(\lambda)$, $\Theta(\lambda)$ and $h(\lambda)$ at any desired wavelength in the 0.35–1.8 μm spectral interval.

Table 2: Selected spectral bands.

	MERIS	ATSR2	SeaWiFS	VGT
Blue	442	–	443	B0
Green	560	550	555	–
Red	665	660	670	B2
NIR	865	870	865	B3

4 CALIBRATION REFERENCE EVALUATION

4.1 Method

The objective of this evaluation is to assess the SEVIRI calibration reference errors and biases. The radiative transfer simulation accuracy is constrained by the assumptions and numerical method of the 6S code as well as the uncertainties of the state variable characterization. The evaluation of this uncertainties relies on the comparison between simulations calibrated space-based measurements acquired by Envisat/MERIS, ERS2/ATSR-2, SeaStar/SeaWiFS and VEGETATION over the SEVIRI desert calibration targets. These instruments have a spatial resolution of about 1 km. For each instrument, TOA reflectances r_f^* were acquired in the blue, green, red and near infrared (NIR) spectral band when available (Table 2). These reflectances are averaged over a 100 km \times 100 km areas centered on each target location but SeaWiFS with an area of about 20 km \times 20 km. The standard deviation $\sigma_{r_f^*}$ of r_f^* over these targets usually does not exceed 2%.

These observations are next systematically simulated accounting for the exact geometry of observation and illumination of each instrument as well as the spectral response of each band. In addition to the simulated TOA reflectance r_f , we also calculated the corresponding simulation error ε_{r_f} based on the estimated state variable characterization error.

The comparisons are based the analysis of the following values:

1. The relative bias $\beta(t, d)$ between the observation $r_f^*(t, d)$ acquired over target d at time t and the corresponding simulation $r_f(t, d)$

$$\beta(t, d) = \frac{r_f^*(t, d) - r_f(t, d)}{r_f(t, d)} \quad (4)$$

2. The bias error $\epsilon_\beta(t, d)$

$$\epsilon_\beta(t, d) = \beta(t, d) \left(\left| \frac{\sigma_{r_f^*}(t, d)}{r_f^*(t, d)} \right| + \left| \frac{\epsilon_{r_f}(t, d)}{r_f(t, d)} \right| \right) \quad (5)$$

3. The monthly mean relative weighted bias $\bar{\beta}_m$ averaged over all 18 targets

$$\bar{\beta}_m = 100 \frac{1}{18} \sum_{d=1}^{18} W_m(d) \sum_{t_m=1}^{N_m(d)} \beta(t_m, d) \frac{1}{\epsilon_\beta^2(t, d)} \quad (6)$$

where $N_t(d)$ is the number of observations available over target d during the month m with $t_m = \{t \in m\}$ and $W_{t_m}(d)$ is equal to

$$W_m(d) = \sum_{t_m=1}^{N_m(d)} \epsilon_\beta^2(t, d) \quad (7)$$

4. The standard deviation $\sigma_{\bar{\beta}_m}$ of $\bar{\beta}_m$.

5. The monthly relative weighted bias $\bar{\beta}_m$ averaged overall all available years for a given month m and is noted $\bar{\beta}_m$

6. The standard deviation $\bar{\sigma}_{\bar{\beta}_m}$ of $\bar{\beta}_m$.

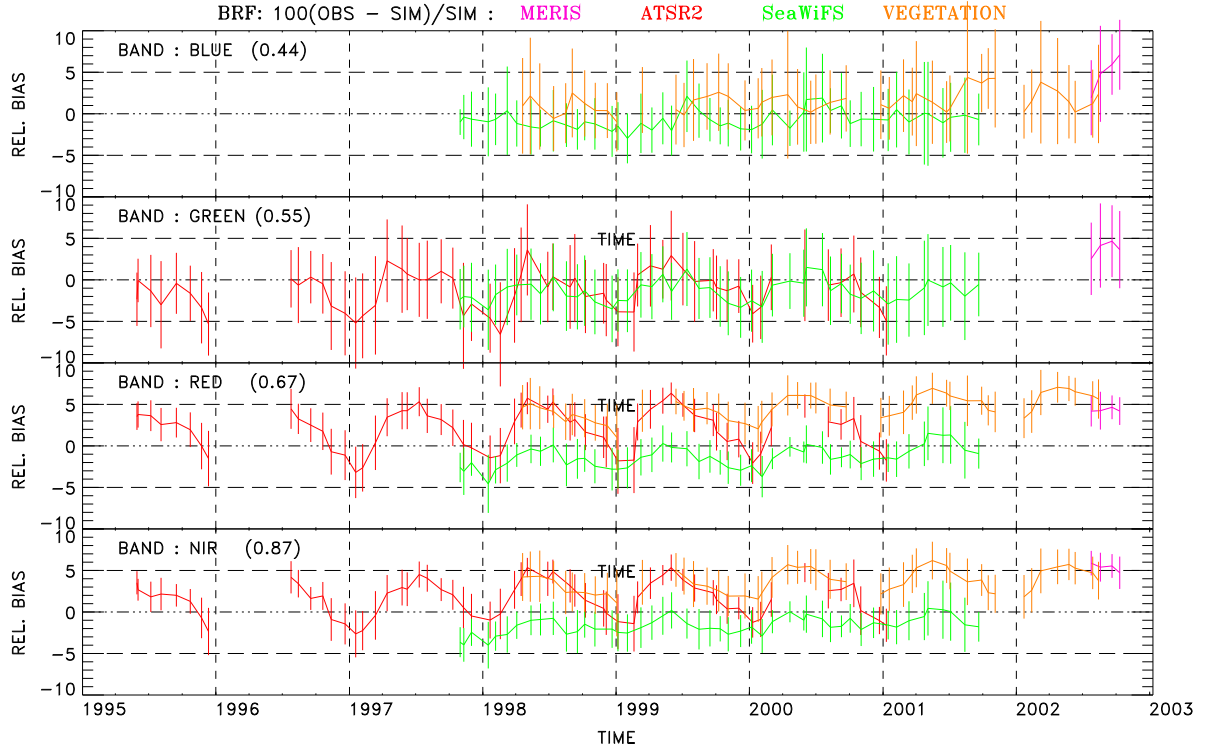


Figure 2: Seasonal trend of the monthly relative bias $\bar{\beta}_m$ in percent between simulations and observations over all targets. The values of $\sigma_{\bar{\beta}_m}$ are shown with the vertical bars.

4.2 Results

Figure (2) shows the monthly mean relative weighted bias for each instrument. As can be seen, the mean bias does not exceed $\pm 6\%$ in all bands, whatever the instrument. The bias exhibits a small seasonal trend of about 3%, which have a similar phase for ATSR2, VEGETATION and SeaWiFS, but which is larger for the former two instruments. Several reasons might explain this seasonal trend. First, uncertainties in the characterisation of the surface anisotropy

and aerosol properties might be responsible for an error that is sensitive to seasonal change of the Sun angle. Second, possible errors of the 6S model should not be excluded. In a recent paper, [7] shows that this model typically agrees within $\pm 4\%$ with other radiative transfer models over non-Lambertian surfaces. Finally, the size of the target might also contribute to this seasonal effect. This effect is far less important for SeaWiFS data which are averaged over a much smaller area than data acquired by the other instruments.

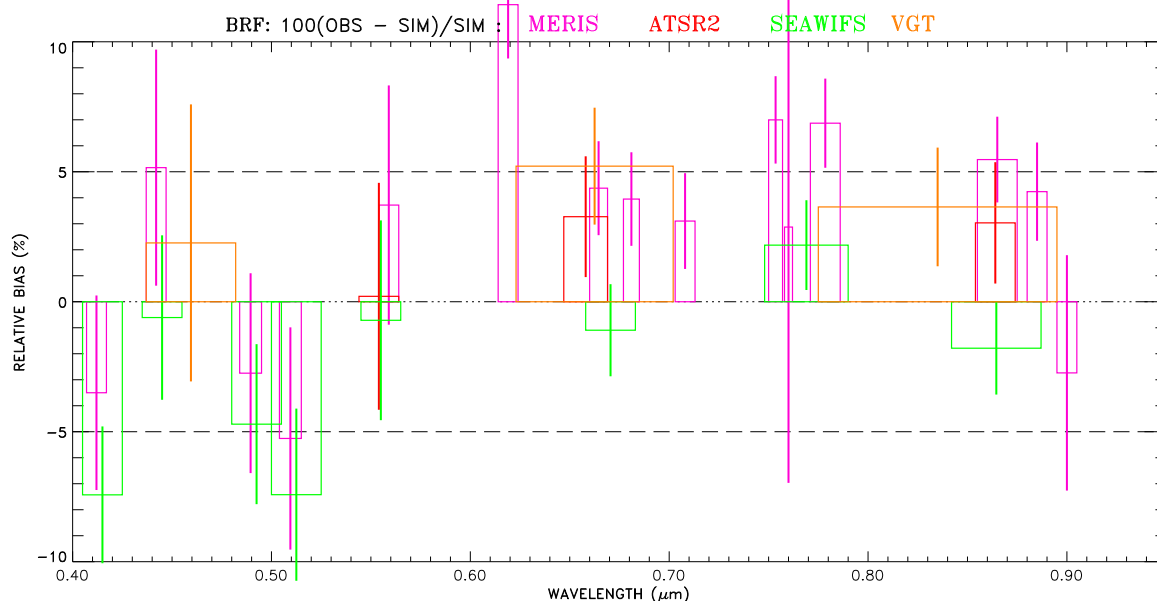


Figure 3: Overall bias $\overline{\beta}_m$ averaged over the months of July, August, September and October

The overall biases $\overline{\beta}_m$ averaged over the months of July, August, September and October are shown on Tables (3) and Figure (3). According to these results, the SEVIRI solar channel calibration reference is very similar to SeaWiFS, to the exception of the 0.4 and 0.5 μm spectral region. MERIS BRFs, as provided by the METRIC software, seem to overestimated by about 5% SeaWiFS ones. ATSR2 and VEGETATION have a very similar radiometric behaviour.

Table 3: Average bias $\overline{\beta}_m$ in percent with respect to the SEVIRI calibration reference for the months of July, August, September and October.

	MERIS	ATSR2	SeaWiFS	VGT
Blue	+5.2%	–	-0.6%	+2.3%
Green	+3.7%	+0.2%	-0.7%	–
Red	+4.4%	+3.3%	-1.1%	+5.2%
NIR	+5.5%	+3.0%	-1.8%	+3.6%

5 CONCLUSIONS AND RECOMMENDATIONS

This paper describes the calibration reference that will be used for the operational vicarious calibration of the SEVIRI solar channels. This reference consists of simulated TOA radiances, using a data set of surface and atmospheric properties. A comparison between calibrated space-borne data and simulations reveals that the relative bias between simulations and calibrated observations do not exceed 6% when a large number of observation are averaged over all targets.

Further efforts are still needed to improve the TAO simulation uncertainties as well as the estimation of the surface anisotropy and aerosol characterization. The use of a radiative transfer code with a rigorous treatment of the multiple scattering between the surface and the atmosphere is also desirable. Finally, it is recommended to extract the BRF over the targets using an area that does not exceed 20km in order not to introduce approximation in the illumination and viewing angles. These results will become more reliable as more MERIS data will be made available.

ACKNOWLEDGEMENTS

POLDER surface BRF and VEGETATION data have been made available by P. Henri and F. Cabot from the French Centre National d'Etudes Spatiales. D. Smith from the Rutherford Appleton Laboratory (UK) collected and processed the ATSR2 data. SeaWiFS data have been prepared by F. Melin from the Joint Research Centre of the European Commission. MERIS data have been processed by L. Bourq from ACRI.

REFERENCES

- [1] A. Arriaga and J. Schmetz. Calibration of the Meteosat-5/-6 VIS channels with help of modelled radiances. *Contributions to Atmospheric Physics*, 72:133–139, 1999.
- [2] I. Chiapello, J. M. Prospero, J. R. Herman, and N. C. Hsu. Detection of mineral dust over the North Atlantic Ocean and Africa with Nimbus 7 TOMS. *Journal of Geophysical Research*, 104:9277–9291, 1999.
- [3] H. Cosnefroy, X. Briottet, M. Leroy, P. Lecomte, and R. Santer. A field experiment in Saharan Algeria for the calibration of optical satellite sensors. *International Journal of Remote Sensing*, 18:3337–3359, 1997.
- [4] H. Cosnefroy, M. Leroy, and X. Briottet. Selection and characterization of Saharan and Arabian desert sites for the calibration of optical satellite sensors. *Remote Sensing Environment*, 58:101–114, 1996.
- [5] Y. M. Govaerts, A. Arriaga, and J. Schmetz. Operational vicarious calibration of the MSG/SEVIRI solar channels. *Advances in Space Research*, 28:21–30, 2001.
- [6] S. B. Hooker and C. R. McClain. The calibration and validation of SeaWiFS data. *Progress in Oceanography*, 45:427–465, 2000.
- [7] A. Lyapustin. Radiative transfer code SHARM-3D for radiance simulations over a non-Lambertian nonhomogeneous surface: intercomparison study. *Applied Optics*, 41:5607–5615, 2002.
- [8] C. Miesch. *Quantification des effets de l'hétérogénéité et du relief d'une scène en télédétection: Modélisation du signal en entrée du capteur*. PhD thesis, ONERA/DOA, 1999.
- [9] B. Pinty, M. M. Verstraete, and R. Dickinson. A physical model for predicting bidirectional reflectances over bare soil. *Remote Sensing of Environment*, 27:273–288, 1989.
- [10] J. M. Renders and S. P. Flasse. Hybrid methods using genetic algorithms for global optimization. *IEEE Transactions on Systems, Man, and Cybernetics*, 26:243–258, 1996.
- [11] J. Schmetz, P. Pili, S. Tjemkes, D. Just, J. Kerkmann, S. Rota, and A. Ratier. An introduction to Meteosat Second Generation. *Bulletin of the American Meteorological Society*, 83:977–992, 2002.
- [12] E. P. Shettle and R. W. Fenn. Models for the aerosols of the lower atmosphere and the effects of humidity variations on their optical properties. Technical Report AFGL-TR-79-0214, U.S. Air Force Geophysics Laboratory, U.S. Air Force Geophysics Laboratory, 1979.
- [13] D. L. Smith, C. T. Mutlow, and C. R. N. Rao. Calibration Monitoring of the Visible and Near-Infrared Channels of Along-Track Scanning Radiometer-2 (ATSR-2) using Stable Terrestrial Sites. *Applied Optics*, 41:515–523, 2002.
- [14] E. F. Vermote, D. Tanré, J. L. Deuzé, M. Herman, and J. J. Morcrette. Second simulation of the satellite signal in the solar spectrum, 6S: An overview. *IEEE Transactions on Geoscience and Remote Sensing*, 35:675–686, 1997.